Available online at www.sciencedirect.com
SCIENCE DIRECT®
Journal of Nuclear Materials 321 (2003) 294–304
journal of nuclear materials
www.elsevier.com/locate/jnucmat

# Density functional study of chemical erosion mechanisms in carbon and boron-doped carbon as plasma facing material in tokamaks

Y. Ferro [a], F. Marinelli [a], A. Allouche [a,*], C. Brosset [b]

[a] *Physique des Interactions Ioniques et Moléculaires, CNRS and Université de Provence (UMR 6633), Campus Universitaire de Saint Jérôme, Service 242, 13397 Marseille cedex 20, France*

[b] *Association Euratom-CEA sur la Fusion contrôlée, CEA/DSM/DRFC, CEA Cadarache, 13108 Saint Paul lez Durance cedex, France*

Received 10 March 2003; accepted 28 May 2003

**Abstract**

Quantum calculations (density functional theory) have been developed in order to propose a new insight into the chemical erosion of pure and doped graphite considered as models for the various carbon materials cladding the first wall of magnetically controlled fusion devices. The elementary processes considered are H, C and $CH_n$ adsorption and desorption, and C, $C_2$, CH, $CCH_n$ extraction from the surface. The quantum results are compared to experiments through tentative new interpretations of the high-resolution electron energy loss spectroscopy vibration spectra, of the thermal desorption spectroscopy experiments and of the analytical models proposed for chemical erosion.


## 1. Introduction

Carbon materials are widely used as plasma facing material cladding the components of the first wall of magnetically controlled fusion devices named tokamaks. They were selected for their low atomic number and their good thermo-mechanical properties. Up to now, carbon-reinforced fiber composite is still foreseen to handle the high heat fluxes, flowing on the divertor target of the future thermonuclear experimental reactor ITER [1]. The drawback of these materials is that they experience erosion when exposed to the hydrogen flux coming from the fusion plasma. Above a threshold energy of about 30 eV, physical sputtering occurs, providing a carbon sputtering yield of about 1% of the incoming hydrogen flux [2]. A complex chemistry between hydrogen and carbon atoms also takes place both at the surface and in the bulk of carbon walls, giving rise to chemical erosion resulting in hydrocarbon production [3]. The rate of chemical erosion can be 10 times more effective than the physical sputtering, depending on the energy range of the incident particles and the temperature of the carbon target.

In his 1995 review, on the hydrogen surface chemistry of carbon as plasma facing material, Küppers [4] proposed a detailed description of the processes behind the interaction of carbon with hydrogen fluxes. These processes were categorized as follows:

(i) $H_2$ release: this was the matter of our previous papers [5–7].
(ii) Atom displacement under H impact: this reaction is produced at very high energies (>124 eV) through kinetic energy transfer to the carbon surface. This can only be investigated by molecular dynamics methods, which is not in the scope of this work.
(iii) Bonding: H particles impinging at the surface can bond to the carbon network, provided that they are slow enough. The result is the hydrogenation and transformation of the carbon surface.
(iv) Etching: various radicals or molecules can be released from the surface thus altered; they can be

* Corresponding author.
*E-mail address:* alain.allouche@piimsdm.univ-mrs.fr (A. Allouche).

0022-3115/$ - see front matter © 2003 Elsevier B.V. All rights reserved.
doi:10.1016/S0022-3115(03)00295-2

injected into the plasma, then be ionized, or be adsorbed again after hydrogenation or de-hydrogenation.

The present work focuses on the last two domains: (iii) and (iv). When carbon surfaces, at temperatures ranging from 500 to 1100 K, are exposed to hydrogen fluxes of thermal energy up to some 10s of eV, relatively complex hydrocarbons can be formed such as $C_2H_y$ and $C_3H_z$ in addition to $CH_x$ [3,8–11]. An experimental study of chemical erosion of carbon exposed to deuterium ion flux, carried out in the tokamak Tore Supra, showed that at $D^+$ energies lower than 50 eV, the carbon production from $C_2D_y$ is as important as that originating from $CD_4$. The $C_3D_z$ contribution is shown to be also significant, since it is only a factor of 3 lower than that of $CD_4$ [12].

In ITER, the hydrocarbon molecule and radical fluxes originating from chemically eroded carbon divertor plates, together with H flux coming from the plasma, are expected to form hydrogen-rich deposited carbon layers on cold surfaces in the divertor area where the ion flux is absent, and also on colder surfaces, not in direct line-of-sight to the plasma, like the pumping ducts [13–15]. This is a critical issue for the future fusion reactor, in which the tritium inventory will have to be controlled for safety reasons.

To develop improved carbon-based materials with reduced chemical erosion, optimized thermo-mechanical properties and reduced hydrogen retention, several doping solutions have been proposed [16], among which boron, which is known for its gettering effect on low $Z$ impurity in tokamaks [17], especially oxygen. Boron doping was shown to enhance the recombinative release of hydrogen in the form of $H_2$, resulting in a reduced thermal-activated erosion yield and a shift of the temperature of the maximum yield to lower temperature. At the same time, hydrogenation of carbon atoms at low temperature does not seem to be influenced [16].

This review is far from being exhaustive but it clearly shows that, in the low-energy range H fluxes, chemical erosion of carbon surfaces involves complex reactions, which have not so far been systematically studied at the nanometer scale, from a theoretical standpoint. As mentioned by Jacob in [18], impinging species in the range of several eV have sufficient energy to break bonds at the surface and to open new reaction channels; this field remains fairly unexplored both theoretically and experimentally. The aim of this work is to model, through the density functional theory, the interaction of small hydrocarbon radicals (–H and $–CH_n$) with the (0 0 0 1) basal plane of pure or B-doped graphite. This substrate is considered as a model for the carbon-based plasma facing materials of tokamaks. The objective of this work is also to thus provide additional quantitative data for analytical kinetics-based models [16,19,20]. Two kinds of phenomena will be considered corresponding to different domains in energy. The very low-energy range reactions (under 5 eV), inducing adsorption/desorption processes and the 10–20 eV range, which is the domain of radical fragments ($CH_n$, $CCH_m$) abstraction from the surface.

The choice of the adsorbed as well as the extracted radicals is not arbitrary. It forms a first attempt to model the chemical reactions possibly occurring on the surface: adsorbed radicals, atom/ion impact induced radicals sputtering, small molecules production induced by abstraction from the surface of $–CH_n$ or $–CCH_n$ fragments will also be considered [21,22]. However, it appears from molecular dynamics simulation that the sputtered hydrocarbon species are mainly $CH_x$ and $C_2H_x$ [23]. All these processes 'activate' the carbon network, either by creating radical sites (H or $–CH_n$ desorption) or by creating vacancy sites (radical abstraction). In the first case, very reactive intermediate species are also injected into the medium above the surface thus reinforcing the reactivity of the whole system. Although these reactive species are very difficult to observe using conventional experimental setups, they play an important role in the chain of reactions leading up to carbon surface erosion.

## 2. Method of computation

In our previous work [5], we established that small clusters can efficiently describe the H–graphite interaction. The smallest of these clusters is displayed in Fig. 1(a) and was referred to as g4. In the present work, we intend to extend the surface relaxation resulting from adsorption processes. Therefore the g4 cluster (16 atoms) is included into a larger system of two layers around g4 on the graphene plane containing 64 atoms (Fig. 1(b)). The whole system is described through the mixed quantum mechanics/molecular mechanics (QM/MM) ONIOM model [24]. The QM/MM approach has

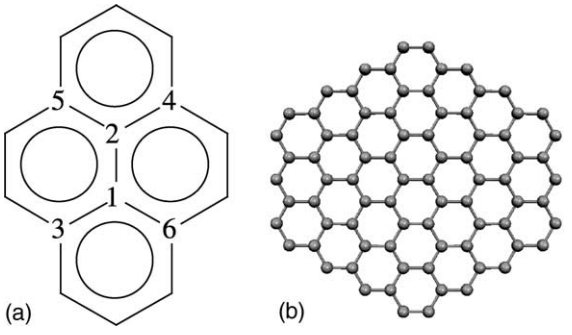


Fig. 1. (a) Reactive, high-level (quantum, B3LYP) part of the cluster; (b) representation of the complete cluster high-level plus low-level (in the ONIOM sense).

been successfully applied to similar carbon systems such as single-walled carbon nano-tubes [25,26]. The high-level cluster (g4) is computed at the UB3LYP/6-31G approximation level. The low-level layer is described through molecular mechanics (MM) and the UFF force field [27]. Whereas in [5] only the adsorbent carbon and its first neighbors were allowed to relax, here the whole system (high-level and low-level clusters) has been optimized. The calculation is performed using the Gaussian 98 computer programs suite [28].

The systems under study are constituted by H atoms or $-CH_n$ radicals, $n = 0$–3, in interaction with the (0 0 0 1) basal plane of graphite. Boron doping is modeled by substitution of $C_1$ (first neighbor, called B1 system in the following) or $C_3$ (second neighbor, B3 system). In any case, the reactive carbon center is always $C_2$ (Fig. 1(a)). Statistically, this model accounts for a doping rate of up to 10% in boron considering that on a graphite surface each carbon has 3 first neighbors and 6 second neighbors. Experimental studies have showed that boron concentration as low as 3% is sufficient to drastically decrease the chemical erosion rate of boron-doped graphite under hydrogen ion flux bombardment [16]. Above a threshold concentration, embedded crystallites structures such as $B_4C$ appear in the carbon matrix. This problem is under investigation and will be developed in a forthcoming paper. The following quantities will be calculated: adsorption/desorption energies of the above-cited reactive species, CH stretch frequencies, surface erosion through abstraction of CH, CC and $CCH_n$ radicals leading to the formation of single holes in the carbon lattice. In the following, we will refer to this species as 'embedded radical'. The whole of these processes corresponds to the definition of swift chemical sputtering, which can occur even when the incoming energy is in the eV range [29].

The adsorption/desorption energy is evaluated as

$$\Delta E = E_{\infty}(\text{graphene} + \text{adspecies}) - E_{\min}(\text{graphene} + \text{adspecies}), \quad (1)$$

where $E_{\min}$ stands for the total energy of the system at its minimum, $E_{\infty}$ is the energy for the admolecule at 5 Å from the graphene, the other geometry parameters remaining unchanged. This approximation assumes that the surface and the radical do not relax after desorption or removal of a fragment creating a carbon vacancy in the surface (non-adiabatic approximation).

In the graphene layer, all the quantum C–C bonds are 1.416 Å long, the MM ones are very similar, 1.409–1.415 Å according to their location in the cluster. This is in good agreement with the $d_{C-C}$ distance in bulk graphite, 1.423 Å [30]. The B-doped graphene remains plane but the C–B bonds are longer than the C–C ones 1.462–1.479 Å, in good agreement with [6] (1.46–1.50 Å) and [31] (1.39–1.70 Å) on hyparene compounds. Doping in the second neighbor, B3 system, induces a shortening of the $C_1$–$C_2$ bond (1.400 Å).

Concerning the in-plane aromatic CH stretching modes, the calculation was performed on benzene, pyrene and coronene aromatic cycles. The associated calculated scaled frequencies are summarized in Appendix A. It can be seen that these modes are quite insensitive to the number of aromatic nuclei.

In the following, we will denote [g4 + C] + H, the system constituted by C bond to g4 and H isolated far from the system described within the brackets, and the equivalent for the other systems considered in the following sections. A special system of reference will be [g4] + C + 3H, i.e. the graphene layer plus one carbon and three hydrogen atoms far from the surface and far from each other.

## 3. Results

### 3.1. Hydrogen atom adsorption

We have calculated an adsorption energy of 0.8 eV (74.3 kJ mol$^{-1}$) for H on the pure graphite model; the corresponding C–H bond length is 1.125 Å. Boron substitution in B1 considerably increases the adsorption energy, 2.2 eV and less dramatically the CH length, 1.132 Å. However, the doping effect rapidly wears off since the substitution in second neighbor position yields 1.0 eV in energy and a bond length of 1.128 Å. The complete optimization of the cluster induces a surface curvature that can be observed in Figs. 2–4. This is inherent to the model, which is finite in dimension and the fact that we did not impose any constraint. It has been shown [32] by photoelectron spectroscopy that the adsorption energy of hydrogen on graphite, single-walled nano-tubes and $C_{60}$ increases with the local curvature. In the present calculation, this does not induce significant perturbation comparing to our previous studies detailed in the next paragraph.

The present ONIOM model confirms the main result of [6]: the substitutional B-doping reinforces the C–H bond. The former results were respectively 0.7 eV for g4, 2.8 eV for B1 and 1.7 eV for B3. It must also be noted that the calculation of the interaction energy is different

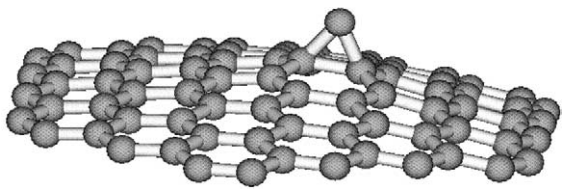

Fig. 2. Stationary geometry for the adsorption of a single carbon atom on the graphene sheet (singlet state).

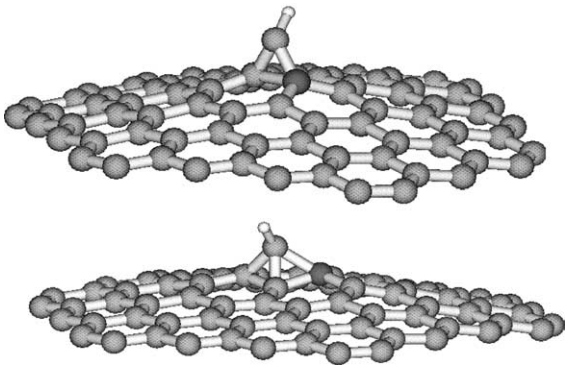

Fig. 3. Stationary geometry for the adsorption of the –CH radical on the first neighbor boron-doped graphene: (a) triplet state, (b) singlet state.

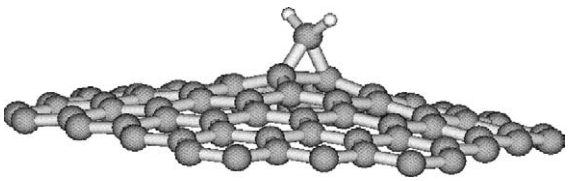

Fig. 4. Stationary geometry for the $–CH_2$ adsorption on graphene.

in the two papers. In [6], the reference state was relaxed whereas here it is frozen. Relaxation of the reference leads to a gain in adsorption energy of about 0.9 eV according to [33]. However, the boron doping effect appears to be the same in both studies except for the long-range behavior that is weaker in our case with B3. This discrepancy can be attributed to the difference in surface relaxation. No constraint was imposed to the interacting system here, leading to an increase in adsorption energy for H (0.8 eV *plus* about 0.9 eV for relaxation of the reference adding up to 1.7 eV, as compared to the 0.7 eV found in [6]). This greater adsorption energy is in agreement with Letardi et al. [34] who have found adsorption energies of 1.7–1.9 eV on extended relaxed periodic graphite models. In any case, the reactive carbon takes on a tetrahedral configuration and hence evolving from $sp^2$ to $sp^3$ hybridization.

The CH vibrator frequency on pure graphene ($\nu_{CH} = 2592$ cm$^{-1}$) is very low compared to the frequencies of the molecular systems given in Appendix A for the C($sp^3$)H vibrational frequencies calculated at the same level of approximation. It reflects the weakness of the bond and the fact that the carbon hybridization is half way between plane $sp^2$ and full tetrahedral $sp^3$. As an illustration, the CCH valence angle is 99.2° whereas it is 109.2° in cyclohexane and 111.3° in ethane.

In B1, the C–H bond length and consequently $\nu_{CH}$ decrease, thus denoting a weakening of the C–H bond. This is in apparent contradiction with the gain in energy of 1.38 eV calculated on B1. This energy gain is probably due to an electronic point of view. The charge transfer observed from B to C in B1 can illustrate this last point. On the H-adsorbed pure graphite model, the Mulliken charge of $C_2$ is −0.39 electron. It becomes −0.47 electron in the B1 system while the boron atom is discharged (+0.24). Usually one expects that the empty boron 2pz orbital will strongly attract the π aromatic electrons and then discharges the neighboring carbons. On the contrary, the electron charge transfer occurs from B to C as it was also shown by Wang et al. [31]. The effect, however insignificant on bare surfaces, does become important on hydrogenated ones, so the C–H bond is much more polarized. This is also related to the molecular orbital analysis developed in paper [6] where we observed that in case of pure graphite, the extra electron brought in by the H atom is located on an antibonding type π orbital, whereas in the B-doped one, due to the fact that boron has one electron fewer than carbon, the H electron can occupy a bonding π orbital.

In B3, the C–H bond length nearly reverts to its initial value (pure surface) and the chemical bond is a little stronger, 2.2 eV (Table 1), which is consistent with the larger frequency calculated. The boron atom no longer acts as electron donor, its charge is 0.01 electron; nevertheless it induces an enrichment of the $C_2$ electron population, which is now −0.51 electron leading again to the polarization of the C–H bond.

The hydrogen atom is never isolated on the surface, in actual fact, up to 40% of the surface carbons are hydrogenated. We then considered four Hs adsorbed on the neighbors of $C_2$: $C_1$, $C_4$ and $C_5$ (Fig. 1(a)). This hypothesis is consistent with [7] where it is showed that the reactivity of these centers is enhanced by the initial H adsorption. For these last three sites, CH remains 1.12 Å but $C_2H$ is now 1.09 Å, i.e. shorter than in cyclohexane or ethane (see Appendix A). The frequencies are 2928 cm$^{-1}$ for $C_2H$ and 2636, 2714 and 2728 cm$^{-1}$ for the other three sites. This blue shift is probably due to a larger relaxation of the layer induced by the change in hybridization of the carbons. This dispersion of the $\nu_{CH}$ signal is confirmed by experimental results reported by Zecho et al. [35] who found, in a 2000 K thermal H atom

Table 1
Adsorption energy (eV) for pure, first neighbor B substitution (B1), second neighbor B substitution (B3)

| | Graphite | B1 | B3 |
|---|---|---|---|
| H | 0.8 | 2.2 | 1.0 |
| C | 3.4 | 2.0 | 2.0 |
| CH | 1.0 | 4.0 | 5.7 |
| $CH_2$ | 3.6 | 4.9 | 4.4 |
| $CH_3$ | 1.4 | 4.2 | 3.1 |

source adsorption experiment on HOPG, a major peak at 2650 $cm^{-1}$, a small satellite at 2380 $cm^{-1}$ and a residual one at 2770 $cm^{-1}$. This was also confirmed by DFT calculations carried out by the same authors.

### 3.2. Carbon atom adsorption

The two most stable electronic configurations for the system [g4 + C] are singlet and triplet. The triplet is 0.1 eV more stable, but in this structure the adsorbed C's electrons are not coupled to those of the graphene, therefore no covalent bond is established, only van der Waals one and the distance to the surface is 2.42 Å. In the singlet state, stability is insured by two covalent bonds making an almost regular cyclic structure (Fig. 2) since the C–C bond lengths are 1.53, 1.54 and 1.59 Å (horizontal bond). The adsorption energy is 3.4 eV. A very similar structure has been found by Nordlund et al. [36] using molecular dynamics. They found 1.49 Å for the upward bonds and 1.56 Å for the horizontal one, their associated binding energy is 3.3 eV.

The B1 boron doping breaks this cycle and the adsorbed carbon is single-bonded to $C_2$ at least in the doublet state. This bond breaking causes adsorption energy to drop down to 2.0 eV. The quartet state is less stable by 0.3 eV, with a cycle analogous to the one shown in Fig. 2, except that the base is $B_1$–$C_2$.

The system B3 does not exist by itself since the adsorbed carbon does not bond to $B_3$ but slips toward $B_1$.

### 3.3. CH adsorption

On the pure surface, the two spin multiplet states, doublet and quartet, are nearly equivalent, the first one being more stable by 0.13 eV, although the C–C bond length is very long (1.62 Å). This system is more stable by 3.4 eV than the former one, i.e. [g4 + C] + H, indeed a single carbon atom adsorbed on the surface is a very attractive site for the ambient hydrogen atom flux.

The boron doping B1 induces very complex structures, a cycle (Fig. 3(a)) for the triplet state and a tri-bonded pyramidal system (Fig. 3(b)) for the singlet, less stable by 0.4 eV. In the latter case, the C–C bonds are 1.46 and 1.62 Å and the C–B bond length is 1.72 Å.

The B3 systems have very similar structures except that the tetragon is based on $C_1C_2C_4$ and no longer involves $B_3$. Compared to the B1 systems, they can be considered as associated local minima about 0.8 eV higher in energy. This underlines the complexity of the problem and the great number of local minima that can be found. These multiple bonds account for the large increase in adsorption energy (Table 1) from g4 (one bond) to B1 (two bonds) to B3 (three bonds).

The calculated stretching CH frequency is 2920 $cm^{-1}$ on pure graphite, identical to that of H surrounding by three others H at 2928 $cm^{-1}$. The doping reinforces the C–H bond and the mode is shifted toward the high-frequency domain (Table 2).

### 3.4. $CH_2$ adsorption

The $CH_2$ radical is adsorbed through a cyclic structure (Fig. 4) on pure graphite. The lattice $C_2$–$C_1$ bond length is 1.62 Å, whereas the other two bonds are C–C = 1.50 Å and C–H = 1.08 Å. This can be compared to cyclopropane where C–C = 1.52 Å and C–H = 1.08 Å. It denotes a covalent chemical bond, as a result the adsorption energy increases strongly. The adsorbed carbon is then $sp^3$ and all its valence electrons are involved in a chemical bond. Therefore, this conformation is very stable even if potentially reactive. The [g4 + $CH_2$] system energy is lower by 6.1 eV than the system [g4 + CH] + H, as it could be expected, the CH radical is very reactive, more so than a single adsorbed carbon.

Again, the doped system exposes two minima: B1 is a triangular cycle based on $B_1C_2$, whereas B3 is also a triangle but the basis is only formed of carbon atoms $C_1C_2$, the most stable is B1 (0.4 eV lower). In both cases, the doping reinforces the graphene–radical bond but has very little influence on the vibrational frequencies.

The CH vibrational frequencies are nearly the same for pure and doped systems (from 3035 to 3136 $cm^{-1}$ – Table 2) and are very close to those in cyclopropane (from 3028 to 3127 $cm^{-1}$).

### 3.5. $CH_3$ adsorption

The methyl group adsorbs in a staggered position with respect to the lattice C–C bonds on any surface, doped or non-doped. This system is 3.6 eV more stable than [g4 + $CH_2$] + H, and the adsorbed $CH_2$ is then less reactive than CH.

Table 2
CH stretch mode frequencies ($cm^{-1}$) for adsorbed radicals

| | Graphite | B1 | B3 |
|---|---|---|---|
| H | Isolated: 2592 Cluster: 2636, 2714, 2728, 2928 | 2460 | 2702 |
| CH | 2920 | 3078 | 3136 |
| $CH_2$ | 3035(s) 3133(a) | 3024(s) 3121(a) | 3038(s) 3136(a) |
| $CH_3$ | 2934(s) 3027(a) 3031(a) | 2938(s) 3056(a) | 2953(s) 3053(a) |
| | | 3043(a) | 3038(a) |

$CH_3$ is not strongly bonded to the surface since its adsorption energy is similar to that of H or CH, at least for the pure graphite. This is reflected by the $C_{graphite}$–$CH_3$ bond length that is longer (1.60 Å) than in ethane or cyclo-hexane (1.54 Å). Nevertheless, this bond is reinforced by doping, and even more so in B1, even if the C–C bond length is longer (1.63 and 1.64 Å).

In the same way as for the former radical, the vibrational frequencies are very slightly perturbed by boron substitution, they are also typical of $C(sp^3)H$ as in cyclohexane, a little higher than in ethane.

### 3.6. Relative stability of the adsorbed species

The upper part of Fig. 5 gives a schematic representation of the interaction energies (according to Eq. (1)) of the fragments adsorbed on the non-substituted graphene. The stability, and hence the reactivity, of these adsorbed radicals is an important parameter in evaluating the stability of the entire carbon surface because it considerably influences the single/double bond carbon ratio ($sp^3/sp^2$). The carbon surface can also 'absorb' or 'release' a large amount of H atoms or ions in addition to the amount of hydrogen trapped into the interior of the carbon bulk. The most tightly bonded are C and $CH_2$. The lower part of Fig. 5 describes the respective stability (gain in energy) of these moieties with respect to a unique common reference, [g4] + C + 3H. As it could be predicted, the most stable is the methyl group, which induces a total stabilization of 14.3 eV. This drawing also indicates that the most reactive species is the CH radical since the capture of an ambient hydrogen atom would give adsorbed $CH_2$ with an energy gain of 6.1 eV. It can also be inferred that when a fragment such as C or $CH_2$ is adsorbed, it constitutes a particularly attractive site for the ambient H and it can be successively saturated until $CH_3$ is reached. Since the methyl is not tightly bonded to the surface, it can be easily detached to produce methane in the gas phase. CH also is slightly bonded, it can be detached by slow H impact and captured to produce $CH_2$.

### 3.7. Abstraction

We have calculated the energy needed to extract the adsorbed species *plus* the adsorbent carbon from the lattice. The radical considered and the corresponding energies are presented in Table 3.

The energy needed to extract a single carbon atom from the lattice is 18.3 eV, which is larger than that for CH (13.0 eV). Indeed, the former case implies the breaking up of an aromatic double bond in place of a single bond. Since the boron atom also breaks the aromatic double bond, the first neighbor doping decreases the energy by a factor 24%; this effect is less observable on B3.

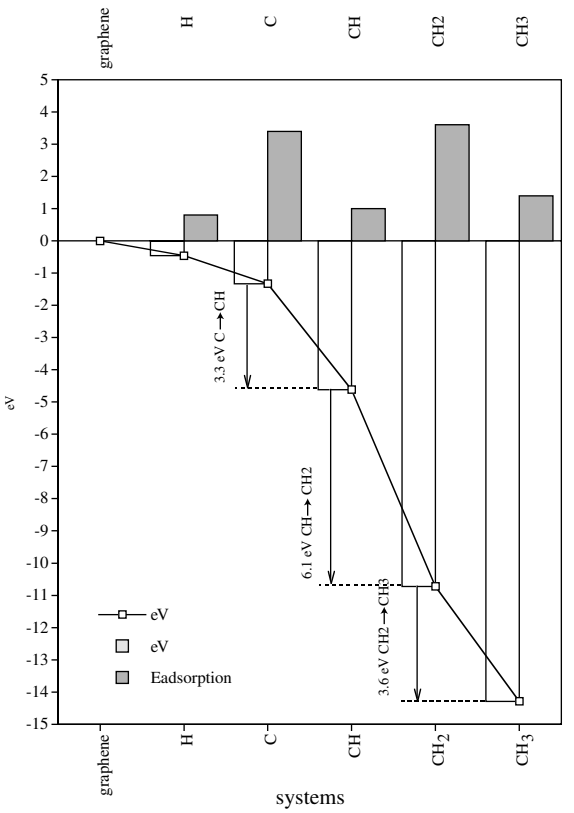


Fig. 5. Summary of the relative stability of the adsorbed radicals. On the upper part is featured the respective adsorption energies. On the lower part are represented the respective stabilities with respect to the common system of reference constituted by the graphene sheet and all the constituents (one carbon, three hydrogen atoms) taken individually. The arrows indicate the amount in energy that would be gained by capturing an extra hydrogen atom.

Table 3
Removing energies (eV) of embedded radicals

| | Graphite | B1 | B3 |
|---|---|---|---|
| C | 18.3 | 13.0 | 15.4 |
| CH | 13.0 | 13.9 | 13.5 |
| $C_2$ | 11.9 | 10.6 | 10.6 |
| CCH | 10.3 | 10.4 | 11.3 |
| $CCH_2$ | 12.3 | 11.3 | 12.4 |
| $CCH_3$ | 13.1 | 11.6 | 9.9 |

The bonding of a carbon atom to the surface also causes the bonding of the $C_2$ atom to the lattice to weaken since the energy needed to remove the embedded CC fragment is lower than the energy needed to remove the CH fragment. The aromatic graphene system is more perturbed by C than by H adsorption. This can also

reflect the greater stability of the CC radical compared to CH.

The CCH embedded radical is also less strongly bonded to the graphene lattice than the other ones, so there is a continuous decreasing in energy from C to CCH with little influence of boron doping. This behavior is inverted with $CCH_2$ and $CCH_3$ as a result of the stability of the formed adspecies. This stability is emphasized by structures and frequencies near cyclohexane or methyl group in the ethane molecule.

Finally, boron doping does not significantly affect the energy needed for abstraction, except for C and $CCH_3$, systems for which it causes a significant decrease.

## 4. General discussion

The general goal of this work was to quantify the energies involved in various model processes of chemical erosion of the pure or B-doped carbon covered inner walls of tokamaks. We intended to underline the complexity of the chemical reactions responsible for this erosion, although the series of radicals we have considered is certainly far from complete. We have shown that a relatively low-energy hydrogen flux (<20 eV) can extract from the carbon surface mono- and double-hydrocarbon radicals and these hydrocarbons can in turn be adsorbed on the surface with energies under 5 eV. In any case, this adsorption process goes along with a trigonalization of the reactive carbon of the surface which becomes $sp^3$ and returns to $sp^2$ after desorption. This particular step, however, was not explicitly considered in this work.

Of course, we had to make number of approximations. The first one was to represent the carbon material used in the PFC by the perfect (0 0 0 1) graphite basal plane and to consider only one layer. We already discussed this point in our earlier paper and we concluded that this model provides a good insight into the elementary chemical processes occurring on real carbon materials. Moreover, having made the choice of a non-defective surface, we cannot take into consideration the border effects, at least in the present paper. We are therefore not able to study reactive sites such as $C(sp^3)H_2$, the only $CH_2$ group we can take into consideration is the adsorbed $C(sp^2)H_2$.

The second approximation lies in the quantum method. We have also shown that the quantum cluster used in this paper (g4) provides reliable results about H adsorption and B doping effects on H adsorption. We have made the substrate relaxation more realistic in taking into account a larger part of the surface through the ONIOM Hamiltonian and we have restricted our study only to first and second boron neighbors, i.e. the substituted atoms that are totally included in the quantum high-level (B3LYP) cluster. However, we have carefully checked that the calculated frequencies were independent of the molecular mechanics part of the cluster. Finally, we have given a non-adiabatic approximation of the adsorption energy, assuming that the surface is not relaxed right after desorption or etching. This seems a reasonable approximation, moreover it is imposed by computational reasons: self-consistency is often not achievable when the quantum system is constituted of two (or more) faraway separated sub-systems; given that, most of the time, complete potential energy surfaces are impossible to build.

It also remains to be noted that the temperature effects cannot be studied since the quantum calculations are performed at 0 K.

### 4.1. Adsorption and abstraction

The present theoretical study confirms that the chemical erosion mechanisms initiated by hydrogen flux in the energy range under 20 eV, coming from the boundary plasma of tokamaks, are complex and involve other species than H only. The impinging H can be adsorbed on the carbon surface, but it can also induce the extraction of numerous radicals from this surface. These radicals can adsorb themselves on the surface or capture ambient hydrogen atoms from the incident flux to generate new radicals that can adsorb in turn on the surface. We have investigated only the simplest of these species, selecting the reactions using only one adsorption or abstraction per radical. A rather similar approach was proposed by Kanai et al. [37]. But in the latter work, the only reactive species considered was H, which upon successive adsorptions leads to the formation of methane.

Schenk et al. [38] have proposed an analytical model for the methane released. They assume that the kinetics is determined by the $C_{lattice}$–$CH_3$ bond breaking associated to an activation energy of 2.43 eV, a value in good agreement with Nakayama et al. [39]. Mech et al. [40] have also provided a model for chemical erosion of graphite due to low-energy $H^+$ and $D^+$ impact. These authors, however, only considered the $-CH_3$ radical adsorption/desorption, and not the other hydrocarbon radicals. It must be pointed out at this stage of the discussion that most of experimental works on chemical erosion mechanisms of graphite or other carbon compounds deal with the production of methane only. In a recent work Zecho et al. [21] propose a mechanism of the hydrogen-induced erosion of unsaturated hydrocarbon molecules. Mech et al. found activation energy of 1.5 eV for the methyl release, and 1.7 eV for H detrapping. Horn et al. [20] have investigated the chemical erosion of C:H film surfaces exposed to thermal H atoms, via hydrocarbon production. Experimental techniques, high-resolution electron energy loss spectroscopy (HREELS) and thermal desorption spectroscopy

(TDS), were used to investigate the films and modeling of hydrogenation, de-hydrogenation thermal decomposition reactions was carried out. In their numerical simulations they used activation energies of 1.95 eV for the erosion step via methyl and 1.73 eV for thermal decomposition reaction of $sp^2$ centers via H split-off. However, these simulations of chemical erosion on a-C:H films are never substantiated by theoretical studies.

There is general agreement on the activation energy for the H released found around 1.7 eV. We found desorption energy of 0.8 eV without relaxing the substrate after desorption, and an estimate of 1.7 eV when relaxation is considered. However, this value is not an activation energy, which is probably 0.2 eV greater [5,41], but the agreement between experiment and calculation is very good.

We found energy of 1.4 eV for $–CH_3$ adsorption. This value is close to activation energies found by Mech et al. [40], and rather close to that of the others authors. However, methane can be produced by desorption (then hydrogenation) of any fragment such as $C_{lattice}–C$, $C_{lattice}–CH$, $C_{lattice}–CH_2$, $C_{lattice}–CH_3$, and the mean value of the corresponding energies (Table 1) is precisely 2.35 eV versus 2.43 eV as found by Schenk et al. [38]. This numerical agreement may be fortuitous, but it is remarkable to observe that our calculations yielded a correct order of energy that can be compared to an experimental value derived from a global empirical approximation. This shows that methane production in TDS experiments or in tokamaks can result from the $C_{lattice}–CH_3$ bond breaking, but also from others $CH_x$ fragments such as CH, whose adsorption energy is close to that of methyl and below the activation energies experimentally established.

Otherwise, no interpretation of acetylene, ethene and ethane production, evidenced notably by TDS experiments, is given in papers such as [38] or similar works. According to our calculation on $CCH_x$ radicals, the surface erosion by chemical sputtering through extraction of an embedded radical is achieved at energies ranging from 10 to 18 eV. These energies can easily be provided to the system by low-energy hydrogen bombardment of the surface. This is consistent with [29] where molecular dynamics calculations established that the chemical sputtering has the highest probability at energies close to 20 eV. It is interesting to notice that the two carbon compounds, CC and CCH especially, are more easily removed than single carbon ones. They can give ethene or acetylene by capture of hydrogen from the incident H flux. The other fragments here considered ($CCH_2$, $CCH_3$) need higher energy. This scheme is also consistent with Vietzke et al. [42] who studied the chemical erosion of a-C:H films by thermal hydrogen atom impact. They detected a large spectrum of hydrocarbons, $–CH_x$, $–C_2H_x$ and $–C_3H_x$. Among them, the most abundant was the $–CH_3$ radical, whereas no $CH_4$ molecule was found. This suggests clearly that the erosion mechanisms in this domain of energy are radical-type chemical reactions.

Roth [3] also has proposed a tentative cataloging of the energy domains concerned by carbon erosion under low-energy hydrogen bombardment. He distinguishes between:

(i) Reaction of thermalized ions within the implanted surface, proceeding via the hydrogenation of carbon atoms.
(ii) Radiation damage induced par kinetic energy transfer to lattice atoms, opening chemical bonds that can afterward be saturated by hydrogen atoms. In our analysis, this corresponds more particularly to abstraction from the surface of embedded radical. These reactions are associated to a threshold energy $E_{dam} \approx 15$ eV, above which damages can be produced under hydrogen bombardment.
(iii) Desorption of hydrocarbon radicals bonded to the surface associated to a threshold of about 2 eV.

The range of values proposed by Roth for the three different reactions mentioned above is very dependent on the nature of the material investigated and the surface temperature. However, the energies that we found for adsorption and abstraction (Tables 1 and 3) are consistent with this scheme.

### 4.2. Effect of Boron doping

The interaction between hydrogen and a large variety of boron-doped graphite or a-C/B:H layers has been extensively studied in many laboratories [43–46]. Their results showed an increase in H retention and a strong decrease of the chemical erosion of graphite together with an increase of desorbed molecular hydrogen during TDS experiments.

Based on experimental considerations, and using ultra-thin amorphous hydrogenated carbon films at boron doping level up to 33%, Schenk et al. [47] have suggested that the activation energy for the C–H bond breaking on B-doped graphite is 2.7 eV. This is very well confirmed by our quantum calculation on B1: 2.2 eV (Table 1). On the contrary, the same authors evaluate the $C–CH_3$ breaking at 2.4 eV under the same conditions. It seems questionable to consider that a C–C bond is weaker than a C–H one, which is why we believe our result to be more likely.

Concerning the adsorption of H, we found that the effect of B-doping is a rather strong stabilization of the bonding on the surface. However the long range effect is more dampened than expected from our previous work [6]. It also stabilizes the $–CH_n$ radicals, and now the effect is at longer distance. In the latter cases, boron

substitution implies complex structures and multiple bonds. Sole the carbon atom is less bonded on the doped surface than on pure graphene, which is due to its single bonding in the former, as opposed to its double bonding in the latter. The best linkage of H and $CH_x$ is consistent with the increase in H retention and the reduced chemical erosion in B-doped carbon films. The efficiency of low boron concentration (as low as 3%) is also consistent with the long-range effect induced by boron.

Schenk et al. invoke the graphitization effect of boron, our investigations are not adapted to this problem, our cluster is too small and a molecular dynamics method on a large system should be more suited and is planned for the next future.

### 4.3. Vibrational frequencies

In 1983, in a pioneer work, Dischler et al. [48] gave a tentative assignment of the infrared absorption bands of amorphous hydrogenated carbon a-C:H. In their sample, 2/3 of the carbon atoms were tetrahedrally coordinated. The observed frequencies were 3300 $cm^{-1}$ assigned to C(sp)H, 3050 $cm^{-1}$ to $C(sp^2)H$ *arom*, 3000 $cm^{-1}$ $C(sp^2)H$ *olef*, 2920 $cm^{-1}$ $C(sp^3)H_2$ *asym* and $sp^3CH$, and 2850 $cm^{-1}$ $C(sp^3)H_2$ *sym*. We are in good agreement concerning the assignment of the CH frequency, their band #7 observed at 2920 $cm^{-1}$ corresponds very precisely with our H or CH (Table 2). In our non-defective model, the $C(sp^3)H_2$ modes are noticeably higher in frequency. This first example underlines the difficulty of assigning the observed infrared adsorption bands or HREELS results making use of the reference of molecular spectra.

Biener et al. [49] have proposed a vibrational frequency assignment in the $\nu_{CH}$ zone for different substrate films: C:H, a-C:H and polyethylene and different vibrational spectroscopies. This work is partly based on [48]. Here, we propose an alternative assignment to Table 1 of Biener's paper, based on our DFT calculations:

- 'Peak code **a**': 3320 $cm^{-1}$ (C:H film) and 3300 $cm^{-1}$ (a-C:H film): can be assigned to an adsorbed –CH radical having a more pronounced sp type than the one derived from our model. This can be due to radical–radical interaction or to surface defects. We did not, however, calculate such a high frequency.
- 'Peak code **b**': 3050 $cm^{-1}$ (C:H film): Biener assigned this peak to aromatic CH. This is in very good agreement with our calculated frequencies (Table 2) on g4, g7 and benzene, but it could also involve a contribution from adsorbed $CH_2$.
- 'Peak code **c**': 2920 $cm^{-1}$ (both C:H film and a-C:H film): corresponds to –H adsorbed aggregated on the surface or to –CH.
- 'Peak code **d**': 2850 $cm^{-1}$ (both C:H film and a-C:H film): the low-frequency peaks are probably due to adsorbed –H in various environments.

These last two vibration mode attributions are to some extent consistent with Biener's, who assigned the last two peaks to respectively anti-symmetric and symmetric $(CH)sp^3$, with no more specification.

Our proposal is in agreement with the HREELS study on thermal treatment presented in the same paper since the first peaks to disappear are those at 3320 $cm^{-1}$, from 300 up to 600 K, then those at 2920 and 2850 $cm^{-1}$ from 600 up to 1040 K: the moieties we associate to these frequencies correspond to the lower adsorption energies (Table 1).

Concerning the HREELS frequencies about boron-doped C:H films in Schenk et al. paper [47], the peak indicated at 3057 $cm^{-1}$ can be attributed to a $–C(sp^2)H$ or to $–CH_3$ as well. Table 2 presents no wave numbers around 2850 or 3315 $cm^{-1}$, neither for pure nor for doped surfaces. In our analysis, the 3315 $cm^{-1}$ peak could be attributed to –C(sp)H adsorbed on surface defects. The 2850 $cm^{-1}$ peak can be attributed to adsorbed –H equivalent to the 2928 $cm^{-1}$ on pure surface since doping causes this frequency to slip down by about 70 $cm^{-1}$.

Also, the B–H frequency near 2500 $cm^{-1}$ cannot be found on the HREELS spectra since we have demonstrated earlier [6] that the protons prefer to bond to carbon, never to boron. Fortunately, this band does not appear, otherwise it could be mistaken with the very low CH stretch frequencies when isolated on the surface at 2592 $cm^{-1}$. The fact this band does not appear also indicates that H adsorption is of cluster-type on the surface.

## 5. Conclusion

In conclusion, even if our model is of limited size, it has been able to evidence some results that can be useful for the general understanding of the physics underlying the chemical erosion of plasma-facing carbon surfaces. In particular, we have shown that these processes are certainly very complex, more than those included in the analytical simulation model. We have determined that boron atom inclusion gives rise to rather complicated chemical reactions. For both surfaces, doped and non-doped, we have been able to propose quantum-based energies associated to already known processes, but also, for reactions seldom included into analytical models. However, the study is developed on a perfect non-defective surface. The next step of the study will be developed on defective surfaces, on carbon atom vacancies and at the borders of the graphene plane, especially the so-called (1 0 1 0) zigzag edge and (1 1 2 1) armchair edge [50].

## Appendix A

CH stretches vibrational frequencies at the UB3LYP/6-31G level (scaling factor: 0.96)

- C(sp)H
  - Acetylene 3311–3416 $cm^{-1}$, $d_{CH} = 1.065$ Å
- C($sp^2$)H
  - Ethylene 3022–3124 $cm^{-1}$, $d_{CH} = 1.087$ Å
  - Benzene 3057–3096 $cm^{-1}$, $d_{CH} = 1.086$ Å
  - Pyrene 3055–3087 $cm^{-1}$, $d_{CH} = 1.086$ Å
  - Coronene 3058–3080 $cm^{-1}$, $d_{CH} = 1.086$ Å
- C($sp^3$)H
  - Ethane 2918–3000 $cm^{-1}$, $d_{CH} = 1.097$ Å
  - Cyclopropane 3028–3127 $cm^{-1}$, $d_{CH} = 1.085$ Å
  - Cyclohexane (chair shaped) 2892–2957 $cm^{-1}$, $d_{CH} = 1.101$ Å

## References


[1] G. Janeschitz, ITER JCT and HTs, J. Nucl. Mater. 290–293 (2001) 1.
[2] W. Eckstein, J. Bohdansky, J. Roth, in: Atomic and Plasma-Material Interaction Data for Fusion, Nuclear Fusion, vol. 1, IAEA, Vienna, 1991, p. 51 (Suppl.).
[3] J. Roth, J. Nucl. Mater. 266–269 (1999) 51.
[4] J. Küppers, Surf. Sci. Rep. 22 (1995) 249.
[5] Y. Ferro, F. Marinelli, A. Allouche, J. Chem. Phys. 116 (2002) 8124.
[6] Y. Ferro, F. Marinelli, A. Allouche, C. Brosset, J. Chem. Phys. 118 (2003) 5650.
[7] Y. Ferro, F. Marinelli, A. Allouche, Chem. Phys. Lett. 368 (2003) 609.
[8] R. Yamada, J. Nucl. Mater. 145–147 (1987) 359.
[9] J.W. Davis, A.A. Haasz, P.C. Stangeby, J. Nucl. Mater. 155–157 (1988) 234.
[10] E. Vietzke, V. Philipps, Fusion Tech. 15 (1989) 108.
[11] A.A. Haasz, J.W. Davis, J. Nucl. Mater. 175 (1990) 84.
[12] A. Cambe, E. Gauthier, J. Hogan, J.M. Layet, J. Nucl. Mater. 313–316 (2003) 364.
[13] A.E. Gorodetsky, I.I. Arkhipov, R.Kh. Zalavutdinov, Yu.N. Tolmachev, S.P. Vnukov, V.L. Bukhoverts, J. Nucl. Mater. 290–293 (2001) 271.
[14] I.I. Arkhipov, G. Federici, A.E. Gorodetsky, C. Ibbott, D.A. Komarov, A.N. Makhantov, A.V. Martin, I.V. Mazul, R. Tivey, A.P. Zakharov, R.Kh. Zalavutdinov, J. Nucl. Mater. 290–293 (2001) 394.
[15] A. von Keudell, T. Schwarz-Selinger, W. Jacob, A. Stevens, J. Nucl. Mater. 290–293 (2001) 231.
[16] C. Garcia-Rosales, M. Balden, J. Nucl. Mater. 290–293 (2001) 173.
[17] J. Winter, J. Nucl. Mater. 176–177 (1990) 14.
[18] W. Jacob, Thin Solid Film 326 (1998) 1.
[19] M. Wittmann, J. Küppers, J. Nucl. Mater. 227 (1996) 186.
[20] A. Horn, A. Schenk, J. Biener, B. Winter, C. Luttterloh, M. Wittmann, J. Küppers, J. Chem. Phys. Lett. 231 (1994) 193; A. Horn, J. Biener, A. Schenk, C. Lutterloh, J. Küppers, Surf. Sci. 331–333 (1995) 178.
[21] T. Zecho, B.D. Brandner, J. Biener, J. Küppers, J. Phys. Chem. B 105 (2001) 6194.
[22] T. Zecho, B.D. Brandner, J. Biener, J. Küppers, J. Phys. Chem. B 106 (2002) 610.
[23] E. Salonen, K. Nordlund, J. Keinonen, C.H. Wu, Contribution Plasma Phys. 42 (2002) 458.
[24] M. Svensson, S. Humbel, R.D.J. Froese, T. Matsubara, S. Sieber, K. Morokuma, J. Phys. Chem. 100 (1996) 19357.
[25] G.E. Froudakis, Nano Lett. 1 (2001) 179.
[26] C.W. Bauschlicher, Chem. Phys. Lett. 322 (2000) 237.
[27] A.K. Rappé, C.J. Casewit, K.S. Colwell, W.A. Goddard, W.M. Skiff, J. Am. Chem. Soc. 114 (1992) 10024.
[28] M.J. Frisch, G.W. Trucks, H.B. Schlegel, G.E. Scuseria, M.A. Robb, J.R. Cheeseman, V.G. Zakrzewski, J.A. Montgomery, Jr., R.E. Stratmann, J.C. Burant, S. Dapprich, J.M. Millam, A.D. Daniels, K.N. Kudin, M.C. Strain, O. Farkas, J. Tomasi, V. Barone, M. Cossi, R. Cammi, B. Mennucci, C. Pomelli, C. Adamo, S. Clifford, J. Ochterski, G.A. Petersson, P.Y. Ayala, Q. Cui, K. Morokuma, D.K. Malick, A.D. Rabuck, K. Raghavachari, J.B. Foresman, J. Cioslowski, J.V. Ortiz, A.G. Baboul, B.B. Stefanov, G. Liu, A. Liashenko, P. Piskorz, I. Komaromi, R. Gomperts, R.L. Martin, D.J. Fox, T. Keith, M.A. Al-Laham, C.Y. Peng, A. Nanayakkara, C. Gonzalez, M. Challacombe, P.M.W. Gill, B. Johnson, W. Chen, M.W. Wong, J.L. Andres, C. Gonzalez, M. Head-Gordon, E.S. Replogle, J.A. Pople, Gaussian 98, Revision A.7, Gaussian, Inc., Pittsburgh PA, 1998.
[29] K. Nordlund, E. Salonen, J. Keinonen, C.H. Wu, Nucl. Instrum. and Meth. B 180 (2001) 77.
[30] P. Trucano, R. Chen, Nature (London) 258 (1975) 136.
[31] Q. Wang, L.Q. Chen, J.F. Annet, Phys. Rev. B 54 (1996) R2271.
[32] P. Ruffieux, O. Gröning, M. Bielman, P. Mauron, L. Schlapbach, P. Gröning, Phys. Rev. B 66 (2002) 245416.
[33] X. Sha, B. Jackson, Surf. Sci. 496 (2002) 318; X. Sha, B. Jackson, D. Lemoine, J. Chem. Phys. 116 (2002) 7158.
[34] S. Letardi, M. Celino, F. Cleri, V. Rosato, Surf. Sci. 33 (2002) 496.
[35] T. Zecho, A. Güttler, X. Sha, B. Jackson, J. Küppers, J. Chem. Phys. 117 (2002) 8486.
[36] K. Nordlund, J. Keikonen, T. Mattila, Phys. Rev. Lett. 77 (1996) 699.
[37] C. Kanai, K. Watanabe, Y. Takakuwa, Phys. Rev. B 63 (2001) 235311.
[38] A. Schenk, J. Biener, B. Winter, C. Lutterloh, U.A. Schubert, J. Küppers, Appl. Phys. Lett. 61 (1992) 2414.
[39] K. Nakayama, S. Fukuda, T. Hino, T. Yamashina, J. Nucl. Mater. 145–147 (1987) 301.
[40] B.V. Mech, A.A. Haasz, J.W. Davis, J. Appl. Phys. 84 (1998) 1655.
[41] L. Jeloaica, V. Sidis, Chem. Phys. Lett. 300 (1999) 157.
[42] E. Vietzke, K. Flaskamp, V. Philipps, G. Esser, P. Wienhold, J. Winter, J. Nucl. Mater. 145–147 (1987) 443.
[43] Y. Hirooka, R. Conn, R. Causey, et al., J. Nucl. Mater. 176&177 (1990) 473.
[44] V.Kh. Alimov, R. Schwörer, B.M.U. Scherzer, J. Roth, J. Nucl. Mater. 187 (1992) 191.
[45] C. Garcia-Rosales, E. Gauthier, J. Roth, R. Schwörer, W. Eckstein, J. Nucl. Mater. 189 (1992) 1.

[46] V. Fernandez, J. Bardon, E. Gauthier, C. Grisolia, J. Nucl. Mater. 196–198 (1992) 1022.
[47] A. Schenk, B. Winter, C. Lutterloh, J. Biener, U.A. Schubert, J. Küppers, J. Nucl. Mater. 220–222 (1995) 767.
[48] B. Dischler, A. Bubenzer, P. Koidl, Solid State Commun. 48 (1983) 105.
[49] J. Biener, A. Schenk, B. Winter, C. Lutterloh, U.A. Schubert, J. Küppers, Surf. Sci. Lett. 291 (1993) L725.
[50] F.H. Yang, R.T. Yang, Carbon 40 (2002) 437.